# Latency Aware Transmission Scheduling for Steerable Free Space Optics

Xiang Sun , *Member, IEEE*, Liangkun Yu , *Graduate Student Member, IEEE*, and Tianrun Zhang, *Graduate Student Member, IEEE* 

Abstract—Free space optics (FSO), which uses light as the carrier to transmit data in free space, has been demonstrated as a secure and high-speed solution for long distance and line-of-sight wireless communications. Applying FSO as fronthaul/backhaul communications between base stations (BSs) and the gateway can significantly increase the fronthaul/backhaul link capacity. Traditionally, the gateway has to be equipped with multiple FSO transceivers, each of which is used to communicate with a BS by establishing a dedicated FSO. In this paper, we propose to use a steerable FSO system, where the gateway is equipped with a steerable FSO transceiver to communicate with multiple FSO transceivers at different BSs in a time division multiplexing manner. Applying the steerable FSO system can reduce the number of FSO transceivers at the gateway, and thus reduce the capital cost of implementing an FSO based fronthaul/backhaul network. We formulate the transmission scheduling problem in the steerable FSO system to optimize the active time for each FSO link associated with the steerable FSO transceiver such that the overall delay of transmitting a packet from geo-distributed BSs to the steerable FSO transceiver at the gateway is minimized, while guaranteeing the latency requirements of the BSs. We propose the laTency aWare transmission Scheduling for sTeerable FSO (TWIST) algorithm, which is designed based on Sequential Quadratic Programming, to efficiently solve the proposed problem. The performance of TWIST is validated via extensive simulations.

Index Terms—Free space optics, steerable, scheduling, queue, delay, sequential quadratic programming

### 1 INTRODUCTION

REE space optics (FSO) is a type of wireless communica- $\Gamma$ tions technology that uses light propagating in free space to convey data wirelessly. As compared to traditional radio frequency (RF) communications, FSO has a higher link capacity [1], lower operational cost [2], lower interference [3], and securer communications [4]. Owing to these advantages, FSO has been applied as a fronthaul and backhaul solution in next generation mobile networks. For example, FSO is applied to achieve high-speed backhaul communications between a macro base station (BS) and a drone mounted BS (DBS) in drone assisted mobile networks, where the DBS is deployed over any place of interests (such as a hotspot or disaster struck area) to relay data between the macro BS and the mobile users [5], [6], [7], [8]. In addition, Curran et al. [9] proposed an FSONet architecture, where different small cell BSs are interconnected together via FSO links to establish a wireless backhaul mesh network. Applying FSO to achieve the communications between a gateway and a BS can provide high link capacity and flexibility to meet the requirements of the mobile network. To enable the gateway to communicate with multiple

BSs, the most common solution is that the gateway can be equipped with multiple FSO transceivers, each of which is used to communicate with a specific BS [10]. For example, as shown in Fig. 1, if three BSs try to communicate with a gateway via the FSO links, the gateway has to be equipped with three FSO transceivers. The gateway equipped with a dedicated FSO transceiver for each associated BS incurs high capital cost, especially when the number of the BSs is large. Also, establishing a dedicated FSO link between a BS and the gateway is not necessary since the capacity of an FSO link is much higher than the data rate requirement of the BS in the access network, especially when the distance between the gateway and the BS is short. In order to reduce the capital cost of FSO based point-to-multipoint communications between the gateway and the BSs, we propose to use a steerable FSO transceiver that can communicate with multiple FSO transceivers in different time slots. Here, a steerable PSO transceiver is an FSO transceiver mounted on a steering gimbal such that the direction of the FSO transceiver can be adjusted by controlling the movement of the steering gimbal. Therefore, as shown in Fig. 1, once the gateway is equipped with a steerable FSO transceiver, it can dynamically switch the direction of its FSO transceiver among the three BSs to communicate with them in different time slots. Note that other methods, such as Galvo Mirrors (GM) [14], digital micromirror devices (DMD) [15], and

Manuscript received 13 June 2021; revised 3 Sept. 2021; accepted 23 Sept. 2021. Date of publication 28 Sept. 2021; date of current version 6 Mar. 2023. This work was supported by the National Science Foundation under Grant OIA-1757207.

(Corresponding author: Xiang Sun.)
Digital Object Identifier no. 10.1109/TMC.2021.3115809

1. Typically, the capacity of an FSO link is around 10 Gbps at a distance of 2 km [11], [12], and the data rate requirement of the access network for a BS is up to 300 Mbps [13]. Thus, the capacity of an FSO link is more than enough to meet the data rate requirement of the access network for a BS.

The authors are with the Department of Electrical & Computer Engineering, University of New Mexico, Albuquerque, NM 87131 USA.
 E-mail: (sunxiang, liangkun, zhangtyrone)@unm.edu.

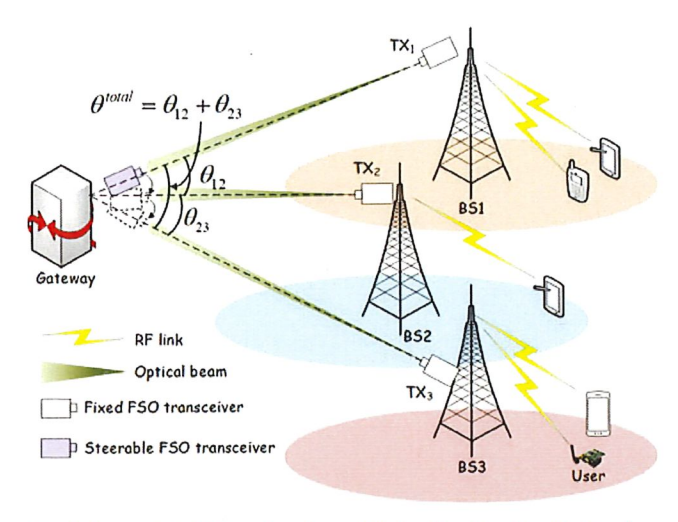


Fig. 1. A steerable FSO system for mobile fronthaul/backhaul networks.

micro-electromechanical systems (MEMS) [16], can also be applied to dynamically steer the optical beams in order to achieve point-to-multipoint communications. However, applying different beam steering methods does not affect the system models and the proposed problem formulation as well as solution later on.

Although applying steerable FSO transceivers at the gateway can reduce the cost, the capacity of the FSO link between the gateway and a BS decreases since the FSO link can only be active (i.e., transmitting data) in a fraction of time when the steerable FSO transceiver at the gateway is pointing to the FSO transceiver at the BS. It is critical to determine the active time of the FSO link between a BS and the gateway since the active time determine the overall throughput of the FSO link. Intuitively, a BS with heavier traffic load will have a longer active time for its FSO link to the gateway. Yet, the duration of the active time for an FSO link is determined by not only the traffic load of the BS but also other factors, such as the achievable data rates of an FSO link, the switching speed of the steerable FSO transceiver, etc. In this paper, we will consider the uplink communications (from different BSs to the gatway) as an example and design a transmission scheduling algorithm to determine the active time of all the FSO links such that the sum of the average delay of transmitting a packet from different BSs to the gateway is minimized, while guaranteeing the QoS of each BS. The contributions of the paper are listed as follows.

- We propose to apply a steerable FSO system to achieve FSO based point-to-multipoint communications for mobile fronthaul/backhaul networks.
- 2) In order to estimate the average delay of an FSO transmitter in processing an incoming packet in the context of a steerable FSO system, we propose a new queuing model, i.e., an M/D/1 queue with periodic vacation (where the length of the vacation is fixed in different scheduling cycles), to model the procedure of an FSO transmitter in buffering and transmitting packets to a steerable FSO receiver, and derive the related queuing delay. The accuracy of the model is demonstrated via simulations.

We formulate the transmission scheduling problem to optimize the active time of the FSO links between the gateway and the associated BSs such that the total average delay of transmitting a packet from the BSs to the gateway is minimized and the QoS of each BS can be satisfied. We propose the laTency aWare transmission Scheduling for sTeerable FSO (TWIST) method to efficiently solve the problem. The performance of the problem is demonstrated via extensive simulations.

The rest of this paper is organized as follows. In Section 2, we briefly introduce the related works. In Section 3, we provide the FSO link capacity model and propose a new queuing model to estimate the average delay of an FSO transmitter/BS in processing a packet. Also, we formulate the transmission scheduling problem to minimize the sum of the average delay of FSO transmitters/BSs in processing a packet, while guaranteeing the latency requirement of the BSs. The TWIST algorithm is proposed and described in Section 4 to efficiently solve the transmission scheduling problem, and the simulation results are analyzed in Section 5. A brief conclusion is drawn in Section 6.

### 2 Related Works

FSO has been adopted as a promising technology to significantly improve the fronthaul/backhaul network capacity in heterogeneous mobile networks [17], [18], [19], [20], [21]. Based on the implementation of steerable FSO transceivers [22], the topology of the FSO based mesh network can be dynamically reconfigured upon requests. Curran et al. [9] optimized the topology and routing paths for a backhaul mesh network, where a number of small cell BSs equipped with steerable FSO transceivers are interconnected with each other via FSO links to forward the data streams between the gateway and small cell BSs. Alzenad et al. [23] proposed an FSO based vertical backhaul/fronthaul framework, where a number of drones equipped with steerable FSO transceivers are cooperative together to establish a mesh network in the air to relay data streams between the gateway and geo-distributed BSs. Based on the proposed framework, Gu et al. [24], [25] designed a method to dynamically reconfigure the topology of the FSO-based vertical backhaul/fronthaul network based on the traffic load of different BSs as well as the states of the FSO links among different drones. Here, topology reconfiguration can be achieved by adjusting the steerable FSO transceivers at different drones. Fan et al. [26] applied the steerable FSO system in gound-to-train communications. Specifically, different railside BSs and a high-speed train are equipped with steerable FSO transceivers. A railside BS can transmit data streams to a high-speed train (which relays the received data to the passengers over WiFi connections) via the established FSO link. The steerable FSO transceivers on the BS and the high-speed train should be well-aligned (when the train moves along the railway) to provide a reliable and broadband FSO link. Also, the steerable FSO transceiver on the high-speed train should be switched to and aligned with the target BS when the train is handed over from the source to the target BS.

Authorized licensed use limited to: UNIVERSITY OF NEW MEXICO. Downloaded on September 15,2023 at 16:24:54 UTC from IEEE Xplore. Restrictions apply.

TABLE 1 Summary of Notations

Motation	Definition
$\mathcal{I}_{m}$	Set of FSO transmitters (TXs) at the BSs
T	Scheduling cycle
$t_i$	Active time of FSO TX i
$\lambda_i$	Average packet arrival rate of FSO TX i
$\mu_{i}$	Packet departure rate of FSO TX i
$\rho_i'$	Utilization of FSO TX i during a scheduling cycle
$ ho_i$	Utilization of FSO TX i during a free period
$ au_i$	Average delay of FSO TX i
$ heta_i^{total}$	Latency requirement of FSO TX i
$\theta^{iout}$	Largest angle among the FSO TXs
ω	Average angle velocity
$\eta_{i}^{tx}$	Optical efficiency of FSO TX i
$\eta^{rx}$	Optical efficiency of the steerable FSO receiver (RX)
$v_{-2}$	Visibility range
$C_n^2$	Atmospheric turbulence strength
Ω	Radius of the aperture in the steerable FSO RX
$rac{\psi_i}{\sigma_i^2}$	Divergence angle of FSO TX i
$\sigma_i^2$	Standard deviation of the beam displacement for
	FSO TX i
ι	Wavelength of the optical beam
κ	Planck constant
$N_b$	Sensitivity of the steerable FSO RX
L	Packet size
$d_i$	Distance from FSO TX i to the FSO RX
γ	Atmospheric attenuation factor
q	Size distribution of the scattering particles
$w_i$	Equivalent beam width of TX i
$h_i^p \ h_i^{atm}$	Pointing error from FSO TX i to the FSO RX
$h_i^{atm}$	Atmospheric attenuation from FSO TX $i$ to the FSO
	RX
$h_i^{tur}$	Atmospheric turbulence from FSO TX i to the FSO
- 000	RX
$h_i^{geo}$	Geometric loss from FSO TX i to the FSO RX
$r_i$	Capacity of the link from FSO TX i to the FSO RX
$N_b$	Sensitivity of the steerable FSO RX
$p_i^{rx}$	Received optical power
$p_i^{rx} \ p_i^{tx}$	Transmission optical power
erf()	Error function, i.e., $\operatorname{erf}(x) = \frac{1}{\sqrt{\pi}} \int_{-x}^{x} e^{-t^2} dt$

The steerable FSO system is also applied to other use cases. Rahman *et al.* [27] explored the FSO based virtual reality (VR) architecture, where a steerable FSO transceiver is used to communicate with a VR headset in motion with its user via an FSO link. They have demonstrated that the throughput of the FSO link can be 40 Gbps or higher, thus satisfying the data rate requirements of various VR applications. Hamedazimi *et al.* [28] proposed the FireFly architecture, which applies FSO to achieve inter-rack communications in a data center. Specifically, each top-of-rack (ToR) switch in a data center is equipped with an FSO transceiver. Different ToR switches communicate with each other by establishing FSO links via ceiling mirrors (which reflect an optical beam from one FSO transceiver to the other).

All the mentioned works use the steerable FSO system to dynamically adjust the FSO based network topology or maintain an FSO link between two endpoints, where the endpoints may move over time. However, to best of our knowledge, none of the works applies the steerable FSO system to achieve point-to-multipoint communications and designs the related scheduling algorithm to minimize the data transmission delay.

3 SYSTEM MODEL

Consider the scenario that multiple BSs (each of which is equipped with a fixed FSO transmitter) try to transmit data streams to the same steerable FSO receiver at the gateway over the FSO links, and Table 1 lists the definitions of the notations used in the paper. Denote  ${\mathcal I}$  as the set of FSO transmitters at the BSs, and i is used to index these FSO transmitters/BSs. Denote T as the duration of a scheduling cycle, in which the steerable FSO receiver receives the data from the FSO transmitters in  $\mathcal I$  based on the round robin manner. That is, during the scheduling cycle T, the steerable FSO receiver initially points to an FSO transmitter in  $\mathcal{I}$  to establish an FSO link, then iteratively switches to the rest of the FSO transmitters in  $\mathcal{I}$  to establish FSO links, and finally switches back to the initial PSO transmitter. For example, as shown in Fig. 1, three FSO transmitters/BSs are trying to communicate with the steerable FSO receiver at the gateway. The steerable FSO receiver would first point to the FSO transmitter at BS1, establish an FSO link, and receive data from the FSO transmitter at BS1. Then, the steerable FSO receiver would iteratively point to the FSO transmitters at BS2 and BS3 to receive data from them. Finally, the steerable FSO receiver would switch back and point to the FSO transmitter at BS1 for a new scheduling cycle. Note that time synchronization among the FSO transmitters and the steerable FSO receiver is very critical to quickly establish the FSO link between the steerable FSO receiver and an FSO transmitter once the steerable FSO receiver is pointing to the FSO transmitter. The existing synchronization solutions, such as Unique-Word [29], can be applied in the proposed steerable FSO system. Denote  $t_i$  as the amount of active time (i.e., communications time) for FSO transmitter i to send data to the steerable FSO receiver at the gateway during a scheduling cycle  $T^2$ . If  $\omega$  is the average angle velocity of the steerable FSO receiver, then we have

$$T = \sum_{i \in \mathcal{I}} t_i + \frac{2\theta^{total}}{\omega},\tag{1}$$

where  $\theta^{total}$  is the largest angle among the FSO transmitters with respect to the steerable FSO receiver. For example, as shown in Fig. 1, three FSO transmitters (i.e.,  $TX_1$ ,  $TX_2$ , and  $TX_3$ ) communicate with the same steerable FSO receiver (denoted as S) at the gateway. Thus, the largest angle  $\theta^{total}$  equals the angle between lines  $TX_1 - S$  and  $TX_3 - S$ , i.e.,  $\theta^{total} = \theta_{12} + \theta_{23}$ . Note that in the three dimensional layout, the FSO transmitters may be in different altitudes, but  $\theta^{total}$  still equals the sum of the angles among all the FSO transmitters and the steerable FSO receiver, and so Eq. (1) is still valid.

# 3.1 Achievable Data Rate of an FSO Link Between a BS and the Gateway

An optical beam transmitted from FSO transmitter i to the steerable FSO receiver over the atmosphere may suffer from various losses. Specifically,

Note that the steerable FSO receiver has to inform the scheduling information (such as the beginning of active time and the amount of active time for each FSO transmitter) to the FSO transmitters once the scheduling is modified.

data transmission delay. scheduling is modified.

Authorized licensed use limited to: UNIVERSITY OF NEW MEXICO. Downloaded on September 15,2023 at 16:24:54 UTC from IEEE Xplore. Restrictions apply.

#### 3.1.1 Atmospheric Attenuation

An FSO signal may be attenuated owing to absorption and scattering from atmospheric molecules and aerosols, and the strength of the atmospheric attenuation from FSO transmitter i to the steerable FSO receiver can be estimated by [30]

$$h_i^{atm} = e^{-\gamma d_i},\tag{2}$$

where  $d_i$  is the distance between FSO transmitter i and the steerable FSO receiver and  $\gamma$  is the atmospheric attenuation factor indicating how much power of an optical beam is attenuated per kilometer over its propagation path in atmosphere. Here,  $\gamma$  can be estimated by [30]

$$\gamma = \frac{3.91}{v} \left( \frac{\iota}{550} \right)^{-q},\tag{3}$$

where v is the visibility range (i.e., the maximum distance that an object can be clearly discerned) in km,  $\iota$  is the wavelength of the optical beam, and q is the size distribution of the scattering particles in the environment, which depends on the visibility range v [30], i.e.,

$$q = \begin{cases} 1.6, & v > 50 \text{ km,} \\ 1.3, & 6 \text{ km} \le v \le 50 \text{ km,} \\ 0.585v^{\frac{1}{3}}, & v < 6 \text{ km.} \end{cases}$$
 (4)

## 3.1.2 Atmospheric Turbulence Induced Fading

The atmospheric turbulence-induced fading is to describe the average faded power induced by both spatial and temporal random fluctuations of refractive index due to temperature, pressure, and wind variations along with the FSO link between a gateway and a BS [31]. Gamma-gamma and lognormal distributions are the two commonly used models to characterize the distribution of the atmospheric turbulence induced fading for an FSO link. Specifically, the log-normal distribution fits the weak-to-moderate turbulent better and the gamma-gamma distribution works in the strong turbulent [32]. Note that using different atmospheric turbulence distribution models will not affect the problem formulation and algorithm design later on. In the paper, the log-normal distribution will be used to model the atmospheric turbulence induced fading.

Denote  $h_i^{tur}$  as the atmospheric turbulence induced fading of the FSO link from FSO transmitter i to the steerable FSO receiver, and the probability density function (PDF) of  $h_i^{tur}$  is [33]

$$p(h_i^{tur}) = \frac{1}{2\sqrt{2\pi}\xi_x} \frac{1}{h_i^{tur}} \exp\left(-\frac{(\ln(h_i^{tur}) + 2\xi_x^2)^2}{8\xi_x^2}\right),\tag{5}$$

where  $\xi_x^2$  is the log-amplitude variance for an optical beam, which can be approximated by

$$\xi_x^2 \approx \frac{1.23C_n^2 \sqrt[6]{k^7 d_i^{11}}}{4}$$
 (6)

Here,  $C_n^2$  is the strength of the atmospheric turbulence, and k is the number of optical waves, i.e.,  $k=2\pi/\iota$ . Thus, the

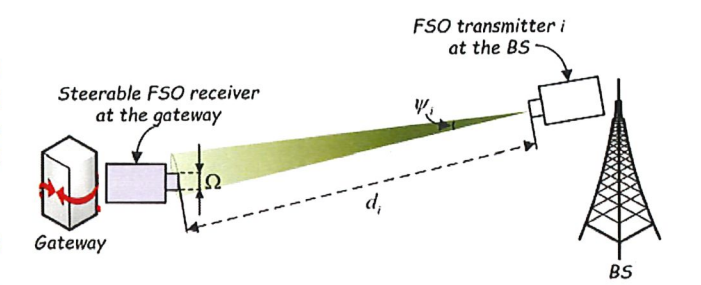


Fig. 2. Parameters of an FSO link.

 $E(h^{tur})$ , is

$$E(h_i^{tur}) = \int_0^1 h_i^{tur} p(h_i^{tur}) dh_i^{tur}$$

$$= \frac{1}{2} - \frac{\operatorname{erf}\left(\frac{\xi_x}{\sqrt{\pi}}\right)}{2}.$$
(7)

#### 3.1.3 Geometric Loss

Geometric loss is caused by the divergence of the optical beam between an FSO transmitter and an FSO receiver, and geometric loss can be estimated by [33]

$$h_i^{geo} = \left[ \operatorname{erf} \left( \frac{\sqrt{2\pi}\Omega}{d_i \psi_i} \right) \right]^2,$$
 (8)

where  $\Omega$  is the radius of the aperture for the steerable FSO receiver at the gateway as shown in Fig. 2,  $\psi_i$  is the divergence angle of FSO transmitter i, and  $d_i$  is the distance between the steerable FSO receiver and FSO transmitter i.

### 3.1.4 Pointing Error

Pointing error is due to the misalignment of the optical beam from FSO transmitter i to the steerable FSO receiver, and pointing error can be estimated by [33]

$$h_i^p \approx \exp\left(-\frac{2\delta_i^2}{w_i^2}\right),$$
 (9)

where  $\delta_i$  is the displacement between the center of beam spot from FSO transmitter i and the center of the lens at the steerable FSO receiver and  $w_i$  is the equivalent optical beam width, i.e.,

$$w_i^2 = \left(\frac{d_i \psi_i}{2}\right)^2 \frac{\sqrt{\pi} \operatorname{erf}(\varrho_i)}{2\psi_i \exp(-\varrho_i^2)}.$$
 (10)

Here,  $\varrho_i = (\sqrt{2\pi}\Omega)/(d_i\psi_i)$ .

Note that the displacement  $\delta_i$  in Eq. (9) is a random variable, whose value depends on the accuracy of the Acquisition, Tracking, and Pointing (ATP) system for each FSO link. Normally, the distribution of  $\delta_i$  is modeled as a Rayleigh distribution [34], i.e.,

$$p(\delta_i) = \frac{\delta_i}{\sigma_i^2} \exp\left(-\frac{\delta_i^2}{\sigma_i^2}\right),\tag{11}$$

where  $\sigma_i$  is the standard deviation of the Rayleigh distribuaverage atmospheric turbulence induced fading, denoted as tion for FSO transmitter i, which is determined by the Authorized licensed use limited to: UNIVERSITY OF NEW MEXICO. Downloaded on September 15,2023 at 16:24:54 UTC from IEEE Xplore. Restrictions apply.

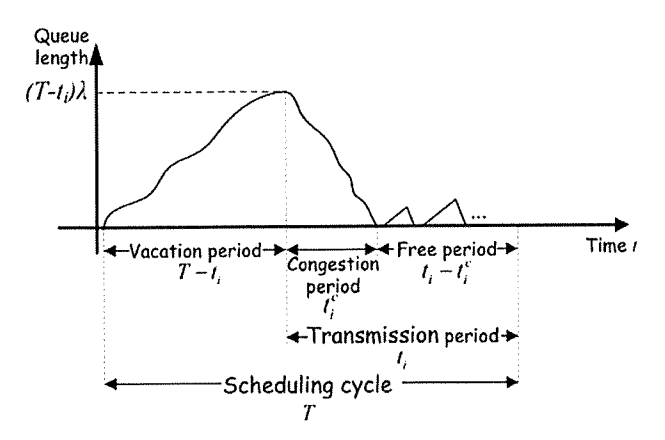


Fig. 3. Illustration of queue length in different periods.

accuracy of the ATP system. Thus, the average pointing error, denoted as  $E(h_i^p)$ , is

$$E(h_i^p) = \int_0^\infty p(\delta_i) h_i^p d\delta_i = \frac{w_i^2}{w_i^2 + 4\sigma_i^2}.$$
 (12)

# 3.1.5 Achievable Data Rate of an FSO Link

The achievable data rate of an FSO link from FSO transmitter i to the steerable FSO receiver at the gateway depends on the received optical power, i.e. [35]

$$r_{i} = \frac{p_{i}^{rx}}{E_{p}N_{b}} = \frac{p_{i}^{tx}h_{i}^{atm}E(h_{i}^{tur})h_{i}^{geo}E(h_{i}^{p})\eta_{i}^{tx}\eta^{rx}}{E_{p}N_{b}},$$
(13)

where  $E_p$  is the photon energy at wavelength  $\iota$  (i.e.,  $E_p = \kappa c/\iota$ . Here,  $\kappa$  is Planck constant and c is the speed of light) and  $N_b$  is the sensitivity of the steerable FSO receiver.

Note that, in the real implementation, the achievable data rate of an FSO link from FSO transmitter i to the steerable FSO receiver at the gateway can be obtained via the field test. But, in the simulations, Eqs. (3), (4), (5), (6), (7), (8), (9), (10), (11), (12), and (13) are used to estimate the achievable data rate of each FSO link, which is one of the input parameters of the proposed optimization problem in Section 3.3.

## 3.2 Average Delay of an FSO Transmitter in Processing a Packet

Each FSO transmitter is associated with a queue to buffer the packets from the users via the BS. Once the steerable FSO receiver is pointing to an FSO transmitter at a BS, the FSO transmitter is active and sends the packets from its queue to the steerable FSO receiver via the FSO link. Assume that the packets arriving at FSO transmitter i's associated queue follows a Poisson distribution, where  $\lambda_i$  is the average packet arrival rate. Meanwhile, when FSO transmitter i is active (i.e., the FSO link is established from FSO transmitter i to the steerable FSO receiver), the service time of FSO transmitter i in transmitting a packet is deterministic, which depends on  $r_i$ , i.e., the achievable data rate of the FSO link from FSO transmitter i to the steerable FSO receiver. Denote  $u_i$  as the packet departure rate of FSO

transmitter *i*'s queue when FSO transmitter *i* is active, i.e.,  $\mu_i = \frac{r_i}{L}$ , where *L* is the average size of a packet.

During a scheduling cycle T, FSO transmitter i comprises two periods, i.e., the transmission and vacation periods. In the transmission period, FSO transmitter i is active and transmitting the packets to the steerable FSO receiver at the gateway. In the vacation period, PSO transmitter i does not transmit packets (i.e., idle), but waits for the steerable FSO pointing to itself. To the best of our knowledge, none of the existing queuing models can be applied to characterize the procedure of FSO transmitter i in buffering and transmitting packets in the context of the steerable FSO system. Thus, we propose a new queuing model, i.e., an M/D/1queue with periodic vacation3 (where the duration of the vacation is fixed in different scheduling cycles) to estimate the average delay of FSO transmitter i. In general, the average delay of PSO transmitter i in processing a packet (denoted as  $\tau_i$ ) includes two parts, i.e., the average queuing delay of a packet waiting in the FSO transmitter i's queue (denoted as  $\tau_i^{queue}$ ) and the average delay of transmitting a packet from FSO transmitter i (denote as  $\tau_i^{tx}$ ). That is,  $\tau_i =$  $\tau_i^{queue} + \tau_i^{tx}$ , where  $\tau_i^{tx} = \frac{1}{\mu_i}$ .

Lemma 1. The average queuing delay of a packet waiting in the FSO transmitter i's queue is

$$\tau_{i}^{queue} = \frac{\rho_{i}^{2}}{2\lambda_{i}(1-\rho_{i})} + \frac{\mu_{i}(T-t_{i})^{2} + \frac{(\rho_{i}^{\prime})^{2}}{1-\rho_{i}}(t_{i}-\rho_{i}^{\prime}T)}{2(\mu_{i}-\lambda_{i})T},$$
(14)

where  $\rho_i = \frac{\lambda_i T}{\mu_i t_i}$  and  $\rho'_i = \frac{\lambda_i}{\mu_i}$ .

**Proof.** proof The average queuing delay of a packet waiting in the FSO transmitter *i*'s queue comprises three parts, i.e.,

 R<sub>i</sub>: the average time of waiting for the packets (which were arrived in previous scheduling cycles) in the queue to be transmitted. The value of R<sub>i</sub> can be estimated based on the M/D/1 queue delay, i.e.,

$$R_i = \frac{\rho_i^2}{2\lambda_i(1 - \rho_i)}. (15)$$

where  $\rho_i$  is the utilization of FSO transmitter i during a scheduling cycle, i.e.,  $\rho_i = \frac{\lambda_i T}{\mu_i t_i}$ .

•  $W_i$ : the average time of waiting for the packets (which were arrived in the current scheduling cycle) in the queue to be transmitted. The whole scheduling cycle can be further divided into three periods, i.e., vacation period  $(T - t_i)$ , congestion

3. In the context of the steerable FSO system, a queue with periodic vacation means that an FSO transmitter may be periodically on and back from the vacation. Here, an FSO transmitter on vacation means that an FSO link is not established between the FSO transmitter and the steerable FSO receiver, and so the FSO transmitter cannot transmit packets from its queue to the steerable FSO receiver. Hence, the packet departure rate for the queue during the vacation period is zero. Similarly, an FSO transmitter back from the vacation implies that an FSO link has been established between the FSO transmitter and the steerable FSO receiver, and so the FSO transmitter is able to transmit packets from its queue to the steerable FSO receiver.

receiver. Denote  $\mu_i$  as the packet departure rate of FSO from its queue to the steerable FSO receiver. Authorized licensed use limited to: UNIVERSITY OF NEW MEXICO. Downloaded on September 15,2023 at 16:24:54 UTC from IEEE Xplore. Restrictions apply.

period  $(t_i^c)$ , and free period  $(t_i - t_i^c)$ , shown in Fig. 3.4 In the vacation period, the arrival packets are accumulated in the queue, and thus the queue length is increasing over time during the vacation period. In the congestion period, the FSO transmitter is active, and so all the packets, which were arrived during the vacation and congestion periods, are transmitted to the steerable FSO receiver. The average queue length during the vacation and congestion periods is  $\frac{(T-t_i)\lambda_i}{2}$ . Also, the average length of the congestion period is  $t_i^c = \frac{(T-t_i)\lambda_i}{u:-\lambda}$ . Finally, in the free period, the arrival packets will be immediately sent to the steerable FSO receiver, which is basically an M/D/1 queuing system, and thus the average queue length during the free period is  $\frac{\rho_i^2}{2(1-\rho_i^2)}$ , where  $\rho_i^\prime$  is the utilization of FSO transmitter i during the free period, i.e.,  $\rho_i' = \frac{\lambda_i}{\mu_i}$ . Hence,  $W_i$  can be estimated by

Based on Lemma 1, we can calculate the average delay of FSO transmitter i in processing a packet based on the following equation.

$$\tau_{i} = \tau_{i}^{queue} + \tau_{i}^{tx} 
= \frac{\rho_{i}^{2}}{2\lambda_{i}(1 - \rho_{i})} + \frac{\mu_{i}(T - t_{i})^{2} + \frac{(\rho_{i}^{\prime})^{2}}{1 - \rho_{i}^{\prime}}(t_{i} - \rho_{i}^{\prime}T)}{2(\mu_{i} - \lambda_{i})T} + \frac{1}{\mu_{i}}.$$
(19)

In order to guarantee the stability of the M/D/1 queue with periodic vacation, the utilization of FSO transmitter iduring a scheduling cycle T should be less than 1, i.e.,

$$\rho_{i} = \frac{\lambda_{i}T}{\mu_{i}t_{i}} < 1 \Rightarrow \rho'_{i}T - t_{i} + \epsilon \leq 0, \tag{20}$$

where  $\epsilon$  is a very small value to enable the inequality to be bounded.

Average queue length when a packet arrives in the vacation and congestion periods 
$$\underbrace{\frac{(T-t_i+t_i^c)}{T}\frac{(T-t_i)\lambda_i}{2}}_{\mu_i} + \underbrace{\frac{t_i-t_i^c}{T}\frac{(\rho_i')^2}{2(1-\rho_i')}}_{\mu_i},$$
(16)

where  $\frac{(T-t_i + t_i^c)}{T}$  and  $\frac{t_i + t_i^c}{T}$  are the probability of a packet arrives during the vacation/congestion period and the free period, respectively. The numerator in Eq. (16) is the average queue length. Plugging  $t_i^c = \frac{(T-t_i)\lambda_i}{\mu_i - \lambda_i}$  into Eq. (16), we have

$$W_{i} = \frac{\lambda_{i}(T - t_{i})^{2} + \frac{(\rho'_{i})^{2}}{1 - \rho'_{i}}(t_{i} - \rho'_{i}T)}{2(\mu_{i} - \lambda_{i})T}.$$
(17)

 $S_i$ : the average time of waiting for the FSO transmitter becoming active. If a packet arrives during the vacation period, it must wait until the FSO transmitter is active. Thus, we have

$$S_i = \frac{T - t_i}{2} \times \frac{T - t_i}{T},\tag{18}$$

where  $\frac{T-t_i}{2}$  is the average time of a packet waiting for FSO transmitter *i* becoming active, and  $\frac{T-t_i}{T}$  is the probability of the packet arriving during the vacation period.

Thus, the average queuing delay of a packet waiting in the FSO transmitter i's queue is  $\tau_i^{queue} = R_i + W_i + S_i$ , which can be further transformed into Eq. (14).

#### 3.3 Problem Formulation

Due to the directional feature of the FSO communications, traditional multiplexing technologies (such as time division multiplexing, frequency division multiplexing, and space division multiplexing), which are widely used in the RFbased point-to-multipoint communications, are unable to be used in the FSO based point-to-multipoint communications. Hence, the steerable FSO system is proposed to adjust the direction of an FSO receiver, thus achieving point-to-multipoint communications. Owing to the characteristic of the steerable FSO system (i.e., each FSO link is periodically inactive owing to the adjustment of the steerable FSO receiver), a new queuing model, i.e., M/D/1 queue with periodic vacation (where the length of the vacation is fixed in different scheduling cycles), is proposed to estimate the latency in the steerable FSO based point-to-multipoint communications. Based on the proposed latency model, we formulate the steerable PSO receiver scheduling problem to minimize the sum of the average delay of transmitting a packet from each FSO transmitter to the steerable FSO receiver, while guaranteeing the QoS in terms of the latency requirement of each FSO transmitter, i.e.,

$$P0: \underset{t_i}{\operatorname{arg\,min}} \sum_{i \in \mathcal{I}} \tau_i, \tag{21}$$

s.t. 
$$\forall i \in \mathcal{I}, \ \tau_i \leq \varphi_i,$$
 (22)

$$\forall i \in \mathcal{I}, \ \rho_i' T - t_i + \epsilon \le 0, \tag{23}$$

where  $\varphi_i$  is the latency requirement of FSO transmitter i, and T is the length of the scheduling cycle defined in Eq. (1). Constraint (22) indicates that the average delay of processing a packet in an PSO transmitter should be no length (i.e., the average number of packets in the queue).

Processing a packet in an FSO transmitter should be Authorized licensed use limited to: UNIVERSITY OF NEW MEXICO. Downloaded on September 15,2023 at 16:24:54 UTC from IEEE Xplore. Restrictions apply.

<sup>4.</sup> Fig. 3 is an intuitive illustration to explain how the average queue length varies in different periods, where x-axis indicates different periods in a scheduling cycle and y-axis represents the average queue

longer than the predefined latency requirement. Constraint (23) ensures the stability of the FSO transmitter i's queue. Note that P0 is the problem formulation for the uplink scenario (i.e., transmitting data from different BSs to the gateway). However, the same problem formulation can be applied to the downlink scenario (i.e., transmitting data from the gateway to different BSs), where  $\tau_i$  and  $\varphi_i$  are the average delay and latency requirement of processing a packet from the steerable FSO transmitter to FSO receiver i, respectively,  $\rho'_i$  is the utilization of the steerable PSO transmitter in transmitting packets to PSO receiver i during the free period (i.e.,  $\rho'_i = \frac{\lambda_i}{\mu_i}$ . Here,  $\lambda_i$  and  $\mu_i$  is the average packet arrival rate and average packet departure rate with respect to the FSO link from the steerable FSO transmitter to FSO receiver i), and  $t_i$  is the active time of the steerable FSO transmitter in sending packets to FSO receiver i during a scheduling cycle T.

# 4 LATENCY AWARE TRANSMISSION SCHEDULING FOR STEERABLE FSO

The objective of P0, i.e.,  $f(t_i) = \sum_{i \in \mathcal{I}} \tau_i$ , is a function of  $t_i$  (according to Eq. (19)). It is easy to derive that the Hessian matrix of the objective function is not semi-definite, and thus P0 is not convex. To tackle this nonconvex problem, we design the laTency aWare transmIssion Scheduling for sTeerable FSO (TWIST) algorithm, which basically applies Sequential Quadratic Programming (SQP) [36]. The basic idea of SQP is to transform P0 into a Quadratic Programming (QP) subproblem in each iteration and solve the QP problem until the algorithm converges to a local minimum. Specifically, let  $\mathcal{L}(t_i, \alpha_i, \beta_i)$  be the Lagrangian function of P0, i.e.,

$$\mathcal{L}(\boldsymbol{t},\boldsymbol{\alpha},\boldsymbol{\beta}) = \sum_{i \in \mathcal{I}} \tau_i + \sum_{i \in \mathcal{I}} \alpha_i (\tau_i - \varphi_i) + \sum_{i \in \mathcal{I}} \beta_i (\rho_i' T - t_i + \epsilon),$$
(24)

where  $\mathbf{t} = \left\{t_1, t_2, \dots, t_{|\mathcal{I}|}\right\}^T$ ,  $\boldsymbol{\alpha} = \left\{\alpha_1, \alpha_2 \cdots \alpha_{|\mathcal{I}|}\right\}^T$ , and  $\boldsymbol{\beta} = \left\{\beta_1, \beta_2 \cdots \beta_{|\mathcal{I}|}\right\}$  are the Lagrangian multipliers. Denote  $t^{(k)}$  as the vector of  $t_i$  in the  $k^{th}$  iteration, i.e.,  $t^{(k)} = \left\{t_1^{(k)}, t_2^{(k)}, \dots, t_{|\mathcal{I}|}^{(k)}\right\}^T$ . Denote  $\boldsymbol{H}^{(k)}$  as the Hessian matrix of the Lagarangian function  $\mathcal{L}(\boldsymbol{t}, \boldsymbol{\alpha}, \boldsymbol{\beta})$  in the  $k^{th}$  iteration. Also, let  $\Delta t^{(k)} = \left\{\Delta t_1^{(k)}, \Delta t_2^{(k)}, \dots, \Delta t_{|\mathcal{I}|}^{(k)}\right\}^T$ , where  $\Delta t_i^{(k)} = t_i - t_i^{(k)}$ . Thus, we construct the following QP problem, which basically reflects the local properties of P0 in the  $k^{th}$  iteration [36].

$$P1: \min_{\Delta t^{(k)}} \frac{1}{2} \Delta t^{(k)}^T H^{(k)} \Delta t^{(k)} + \nabla \left( \sum_{i \in \mathcal{I}} \tau_i^{(k)} \right) \Delta t^{(k)}, \tag{25}$$

s.t. 
$$\forall i \in \mathcal{I}, \nabla \left(\tau_i^{(k)} - \varphi_i\right) \Delta t_i^{(k)} + \tau_i^{(k)} - \varphi_i = 0,$$
 (26)

$$\forall i \in \mathcal{I}, \nabla \left( \rho_i' T - t_i^{(k)} + \epsilon \right) \Delta t_i^{(k)} + \rho_i' T - t_i^{(k)} + \epsilon = 0, \tag{27}$$

where the objective function is the  $2^{nd}$  order Taylor expansion of the objective function in P0, and Constraints (26) and (27) are the  $1^{st}$  order Taylor expansion of Constraints (22) and (23) in P0, respectively, during the  $k^{th}$  iteration. P1 can be solved by the quasi-Newton method [37] to derive the optimal solution  $\Delta t^{(k)}$ , which basically indicates the search direction for t in the next iteration. Specifically, based

on the Karush-Kuhn-Tucker (KKT) conditions, we have the following Jacobian equation [38].

$$\begin{bmatrix} H^{(k)} \nabla \mathbf{g_1} (\mathbf{t}^{(k)}) \\ \nabla \mathbf{g_1} (\mathbf{t}^{(k)}) 0 \\ \nabla \mathbf{g_2} (\mathbf{t}^{(k)}) 0 \end{bmatrix} \begin{bmatrix} \Delta t^{(k)} \\ \Delta \boldsymbol{\alpha}^{(k)} \\ \Delta \boldsymbol{\beta}^{(k)} \end{bmatrix}$$
$$= - \begin{bmatrix} \nabla \mathcal{L} (t^{(k)}, \boldsymbol{\alpha}^{(k)}, \boldsymbol{\beta})^{(k)^T} \\ \mathbf{g_1} (\mathbf{t}^{(k)})^T \\ \mathbf{g_2} (\mathbf{t}^{(k)})^T \end{bmatrix}, \tag{28}$$

 $\rho'_{|\mathcal{I}|}T - t_{|\mathcal{I}|} + \varepsilon$ , and  $\nabla \mathbf{g_1}(\mathbf{t})$  and  $\nabla \mathbf{g_2}(\mathbf{t})$  are the Jacobian matrices of  $\mathbf{g_1}(\mathbf{t})$  and  $\mathbf{g_2}(\mathbf{t})$ , respectively. By solving Eq. (28), the optimal solutions of P1, i.e.,  $\Delta t^{(k)}$ ,  $\Delta \alpha^{(k)}$ , and  $\Delta \beta^{(k)}$ , can be obtained to update t,  $\alpha$ , and  $\beta$  in the next iteration, i.e.

$$\mathbf{t}^{(k+1)} = \mathbf{t}^{(k)} + \Delta \mathbf{t}^{(k)},$$

$$\boldsymbol{\alpha}^{(k+1)} = \boldsymbol{\alpha}^{(k)} + \Delta \boldsymbol{\alpha}^{(k)},$$

$$\boldsymbol{\beta}^{(k+1)} = \boldsymbol{\beta}^{(k)} + \Delta \boldsymbol{\beta}^{(k)}.$$
(29)

Meanwhile, the Hessian matrix of the Lagrangian function can be updated based on the Broyden-Fletcher-Goldfarb-Shanno (BFGS) algorithm [39], i.e.,

$$\mathbf{H}^{(k+1)} = \mathbf{H}^{(k)} + \frac{\mathbf{q}^{(k+1)} \mathbf{q}^{(k+1)^T}}{\mathbf{q}^{(k+1)^T} \Delta \mathbf{t}^{(k)}} - \frac{\mathbf{H}^{(k)} \Delta \mathbf{t}^{(k)} \Delta \mathbf{t}^{(k)^T} \mathbf{H}^{(k)^T}}{\Delta \mathbf{t}^{(k)} \Delta \mathbf{t}^{(k)}}, \tag{30}$$

where

$$q^{(k+1)} = \nabla \mathcal{L}\left(\mathbf{t}^{(k+1)}, \boldsymbol{\alpha}^{(k+1)}, \boldsymbol{\beta}^{(k+1)}\right) - \nabla \mathcal{L}\left(\mathbf{t}^{(k)}, \boldsymbol{\alpha}^{(k)}, \boldsymbol{\beta}^{(k)}\right). \tag{31}$$

Based on the updated values of  $t^{(k+1)}$ ,  $\alpha^{(k+1)}$ ,  $\beta^{(k+1)}$ , and  $H^{(k+1)}$ , a new QP problem will be formulated and solved in the k+1 iteration. The iteration continues until the algorithm converges into a local optimal, i.e.,  $\|\Delta t^{(k)}\| \leq \varsigma$ , where  $\varsigma$  is the predefined convergence threshold. TWIST is summarized in Algorithm 1.

# Algorithm 1. TWIST

Initialize  $\boldsymbol{\alpha}^{(0)}$ ,  $\boldsymbol{\beta}^{(0)}$ ,  $\boldsymbol{t}^{(0)}$ , and  $\boldsymbol{H}^{(0)}$ . k=1. while  $\|\Delta t^{(k)}\| > \varsigma$  do Construct a QP problem, i.e.,  $\boldsymbol{P1}$ ; Derive  $\Delta t^{(k)}$ ,  $\Delta \boldsymbol{\alpha}^{(k)}$ ,  $\Delta \boldsymbol{\beta}^{(k)}$  by solving Eq. (28); Update  $t^{(k+1)}$ ,  $\boldsymbol{\alpha}^{(k+1)}$ ,  $\boldsymbol{\beta}^{(k+1)}$  based on Eq. (29); Update  $\boldsymbol{q}^{(k+1)}$  based on Eq. (31); Update  $\boldsymbol{H}^{(k+1)}$  based on Eq. (30); k=k+1; end

#### 5 SIMULATIONS

the optimal solution  $\Delta t^{(k)}$ , which basically indicates the We conduct extensive simulations to validate the accuracy search direction for t in the next iteration. Specifically, based of the derived average delay model (i.e., Eq. (19)) for the Authorized licensed use limited to: UNIVERSITY OF NEW MEXICO. Downloaded on September 15,2023 at 16:24:54 UTC from IEEE Xplore. Restrictions apply.

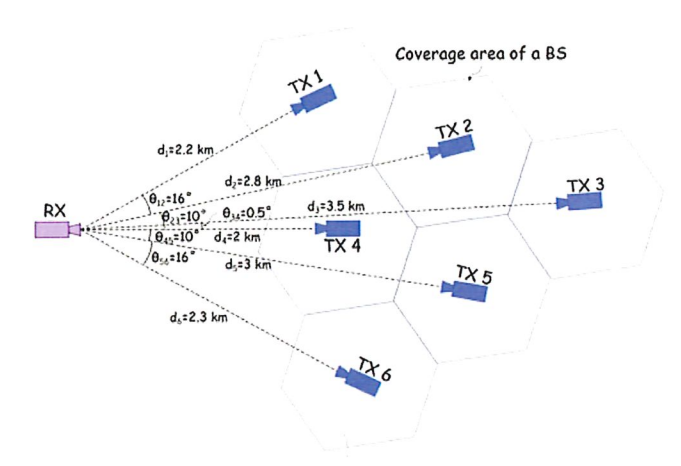


Fig. 4. Simulation setup.

M/D/1 queue with periodic vacation and the performance of TWIST. Assume that there are 6 adjacent BSs, each of which is equipped with an FSO transmitter to transmit their data streams to the gateway. The gateway is equipped with a steerable FSO receiver to receive the data from different BSs in different time slots. The distances and angles between the FSO transmitters at the BSs and the steerable FSO receiver at the gateway are illustrated in Fig. 4. Note that although Fig. 4 shows a 2D layout, the distances and angles in the figure indicate the values in a 3D plane. All the FSO transmitters (i.e., BSs) have the same latency requirement, i.e.,  $\varphi_i = 300$  ms; however, they have different packet arrival rates and we assume that  $\lambda_1 = \lambda_4 = \lambda_6 = 6300 \times \zeta$ packets/s,  $\lambda_2 = \lambda_5 = 4200 \times \zeta$  packets/s, and  $\lambda_3 = 2800 \times \zeta$ packets/s, where  $\zeta$  is the parameter to adjust the packet arrival rates of different PSO transmitters/BSs. Other simulation parameters are listed in Table 2.

# 5.1 Accuracy of the Average Queuing Delay Model

In order to validate the accuracy of the derived average delay model in Eq. (19), we use Matlab Simulink to emulate the process of a steerable FSO receiver iteratively receiving packets from four FSO transmitters. Assume that the steerable FSO receiver at the gateway is serving/connecting four

TABLE 2 Simulation Parameters

Parameter	Value
Transmission power of TX $i(p_i^{tx})$	3 mW[11]
Optical efficiency of TX $i(\eta_i^{tx})$	0.92
Optical efficiency of the FSO receiver $(\eta^{rx})$	0.5
Visibility range (v)	25 km
Atmospheric turbulence strength ( $C_n^2$ )	$10^{-13}m^{-2/3}$
Aperture radius of the FSO receiver $(\Omega)$	42.5 mm[12]
Divergence angle of TX $i(\psi_i)$	0.125 mrad[12]
Standard deviation of the displacement	$0.0001 \ m^2$
$(\sigma_i^2)$	
Wavelength of the optical beam (ι)	1550 nm
Planck constant $(\kappa)$	$6.626 \times 10^{-34}$
	m <sup>2</sup> kg/s
Sensitivity of the FSO receiver $(N_b)$	33067 photons/bit
Average angle velocity (ω)	240 degree/s
Packet size (L)	9000 Bytes

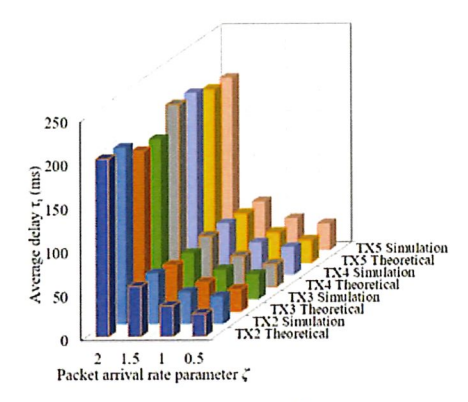


Fig. 5. Accuracy of the average delay model.

FSO transmitters/BSs (i.e., TXs 2, 3, 4, and 5), and Fig. 5 shows the theoretical and simulated average delay of the four FSO transmitters in processing a packet over different values of  $\zeta$  (i.e., different packet arrival rates). The simulated average delay is almost the same as the theoretical value for each FSO transmitter under different packet arrival rates. The average percentage errors of the four FSO transmitters are 1.68% 0.737%, 1.68%, and 1.81%, respectively. Hence, we conclude that the average delay model in Eq. (19) can accurately estimate the average delay of an FSO transmitter in processing a packet.

#### 5.2 Performance of TWIST

Two baseline scheduling algorithms, i.e., round robin (RR) and weighted round robin (WRR) [40], are used to compare the performance of TWIST.

In RR, the active time of all the FSO transmitters is the same, i.e.,  $t_1=t_2=\cdots=t_{|\mathcal{I}|}=t$ . That is, the steerable FSO receiver connects to the first FSO transmitter for t time period to receive packets from the FSO transmitter, and then connects to the next FSO transmitter for another t time period. After the steerable FSO receiver connects to the last FSO transmitter for t time period, it goes back and connects to the first FSO transmitter for a new scheduling cycle. In order to guarantee the stability of the queues in all the FSO transmitters,  $\rho_i'T-t+\epsilon \leq 0$ ,  $\forall i \in \mathcal{I}$ , where  $T=|\mathcal{I}|t+\frac{2\theta^{max}}{\omega}$ . That is,  $\forall i \in \mathcal{I}$ ,  $t \geq \frac{2\theta^{max}}{1-|\mathcal{I}|\rho_i'}$ , Thus, in RR, the active time of

all the FSO transmitters is selected to be  $t_i = t = \max\left\{\frac{2g^{max}}{\frac{\omega}{\alpha} - p'_i + \epsilon}{1 - |\mathcal{I}| \rho'_i} | \forall i \in \mathcal{I}\right\}$ .

In WRR, the active time of the FSO transmitters are proportional to their associated weights, which equals their packet arrival rates. That is, an FSO transmitter with a higher packet arrival rate will have longer active time than an FSO transmitter with a lower packet arrival rate, i.e.,  $t_1$ :  $t_2$ :...: $t_{|\mathcal{I}|} = \lambda_1 : \lambda_2 : ...: \lambda_{|\mathcal{I}|}$ . Similarly, in order to guarantee the stability of the queues in all the FSO transmitters,  $\rho_i'T - t + \epsilon \leq 0$ ,  $\forall i \in \mathcal{I}$ , where  $T = \sum_{i \in |\mathcal{I}|} t_i + \frac{2\theta^{max}}{\omega}$ . Then, we have  $t_i = \lambda_i \times \max\left\{\frac{2\theta^{max}}{\omega} + \sum_{j \in |\mathcal{I}| \setminus i} t_j + \epsilon + \frac{2\theta^{max}}{\omega}\right\}$ .

Assuming the steerable FSO receiver is serving TXs 2, 3, 4, and 5, Figs. 6 and 7 show the average delay of each FSO transmitter and the total average delay of the FSO transmitters, respectively, incurred by TWIST, RR, and WRR under to September 15 2023 at 16:24:54 UTC from IEEE Xolore. Restrictions apply.

Authorized licensed use limited to: UNIVERSITY OF NEW MEXICO. Downloaded on September 15,2023 at 16:24:54 UTC from IEEE Xplore. Restrictions apply

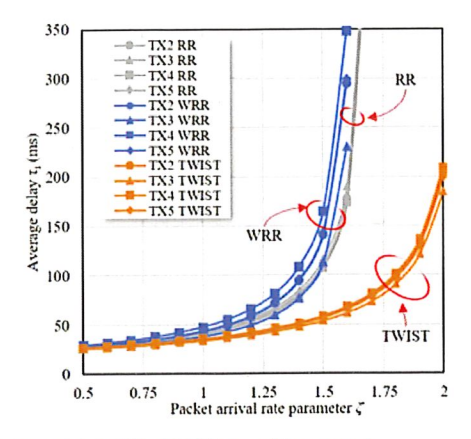


Fig. 6. Average delay of the FSO transmitters over  $\lambda_i$ .

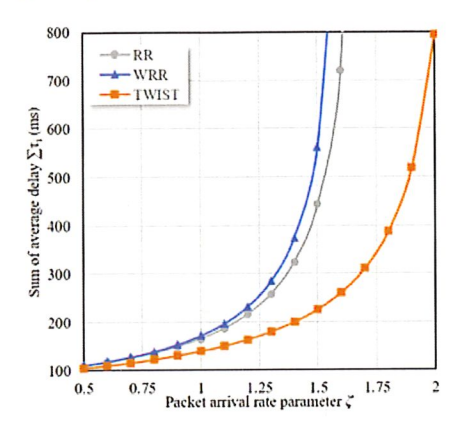


Fig. 7. Total average delay over  $\lambda_i$ .

different traffic loads in terms of packet arrival rates. Note that adjusting  $\zeta$  indicates changing packet arrival rates (i.e.,  $\lambda_i$ ) of the four FSO transmitters. From the figures, we can find that TWIST always incurs the lowest average delay for each FSO transmitter and the lowest total average delay among all the scheduling algorithms. Also, as shown in Fig. 7, the difference of the total average delay between TWIST and WRR/RR increases as  $\zeta$  (i.e., the average arrival rates) increases. In addition, as shown in Fig. 6, TWIST can always generate a feasible scheduling, which guarantees both the stability requirement (i.e., Constraint (23)) and the average delay requirement (i.e., Constraint (22)) for the four FSO transmitters, under different  $\zeta$ . Yet, RR and WRR are unable to find a feasible scheduling when  $\zeta > 1.6$ , which also demonstrates TWIST outperforms WRR and RR.

Assuming the steerable FSO receiver is serving TXs 2, 3, 4, and 5, and  $\zeta=1$  (i.e.,  $\lambda_3=6300$  packets/s,  $\lambda_2=\lambda_5=4200$  packets/s, and  $\lambda_4=2800$  packets/s), we further analyze how the latency requirement affects the performance of TWIST, RR, and WRR. Fig. 8 shows the average delay of all the FSO transmitters by varying the latency requirement of FSO transmitter TX3, i.e.,  $\varphi_3$ . As shown in the figure, TWIST can dynamically adjust the active time of the FSO transmitters to guarantee their latency requirement. Yet, WRR and RR are unable to adjust the scheduling as  $\varphi_3$  varies, and thus the latency requirement of TX3 cannot be satisfied when  $\varphi_3 < 38$  ms. Fig. 9 shows the total average delay of the four FSO transmitters by varying  $\varphi_3$ . We can see that RR/WRR incurs a lower total average delay than TWIST

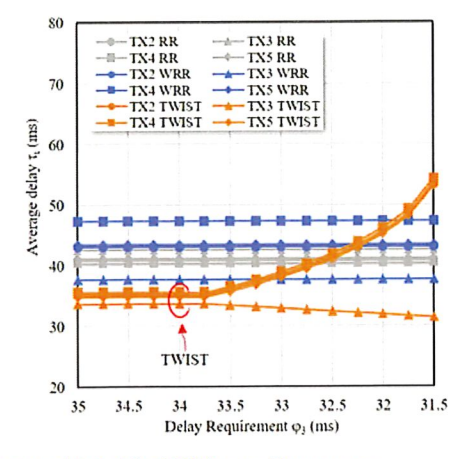


Fig. 8. Average delay of the FSO transmitters over  $\varphi_3$ .

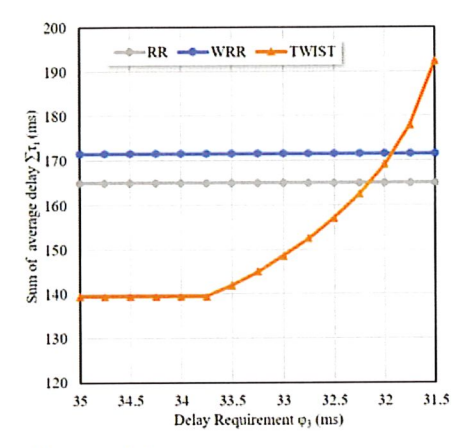


Fig. 9. Sum of average delay over  $\varphi_3$ 

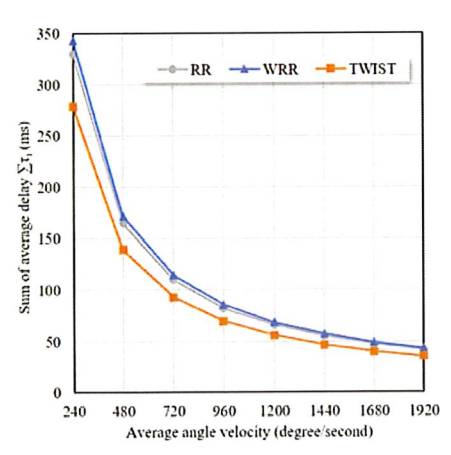


Fig. 10. Sum of average delay over  $\omega$ .

when  $\varphi_3$  is lower than 32/31.7 ms. This is because TWIST tries to guarantee the latency requirements of all the FSO transmitters, and so if TX3 has a low latency requirement, TWIST has to increase the active time of TX3 (i.e.,  $t_3$ ), which may exponentially increase the average delay of the other FSO transmitters. As a result, the total average delay incurred by TWIST exponentially increases.

the four FSO transmitters by varying  $\varphi_3$ . We can see that Assuming  $\zeta=1$ ,  $\varphi_i=300$  ms, and the steerable FSO transmitters by varying  $\varphi_3$ . We can see that Assuming  $\zeta=1$ ,  $\varphi_i=300$  ms, and the steerable FSO transmitters by varying  $\varphi_3$ . We can see that Assuming  $\zeta=1$ ,  $\varphi_i=300$  ms, and the steerable FSO transmitters by varying  $\varphi_3$ . We can see that Assuming  $\zeta=1$ ,  $\varphi_i=300$  ms, and the steerable FSO transmitters by varying  $\varphi_3$ . We can see that Assuming  $\zeta=1$ ,  $\varphi_i=300$  ms, and the steerable FSO transmitters by varying  $\varphi_3$ . We can see that Assuming  $\zeta=1$ ,  $\varphi_i=300$  ms, and the steerable FSO transmitters by varying  $\varphi_3$ . We can see that Assuming  $\zeta=1$ ,  $\varphi_i=300$  ms, and the steerable FSO transmitters by varying  $\varphi_3$ . We can see that Assuming  $\zeta=1$ ,  $\varphi_i=300$  ms, and the steerable FSO transmitters by varying  $\varphi_3$ . We can see that Assuming  $\zeta=1$ ,  $\varphi_i=300$  ms, and the steerable FSO transmitters by varying  $\varphi_3$ . We can see that Assuming  $\zeta=1$ ,  $\varphi_i=300$  ms, and the steerable FSO transmitters by varying  $\varphi_3$ . We can see that  $\zeta=1$  and  $\zeta=1$ 

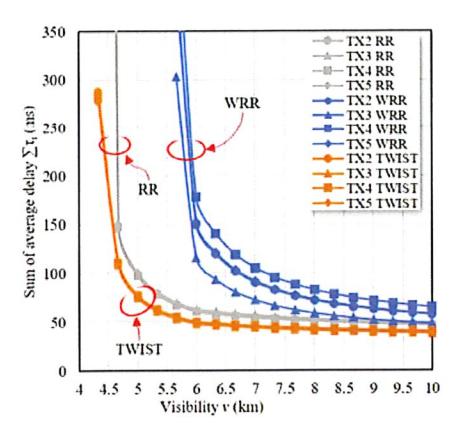
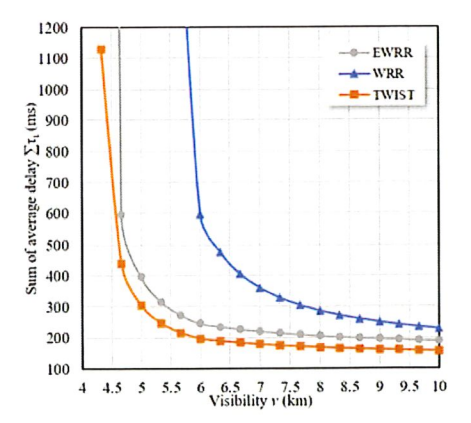


Fig. 11. Average delay over the visibility range.

average delay of the four FSO transmitters by varying the average angle velocity  $\omega$ . Obviously, increasing  $\omega$  can significantly reduce the total average delay incurred by TWIST, RR, and WRR, and the performance gap between TWIST and RR/WRR increases as  $\omega$  increases. Thus, it is promising to apply GM, DMD, and MEMS, which are the solutions (mentioned in Section 1) to steer the optical beams much faster (i.e., larger  $\omega$ ).

As discussed in Section 3, the visibility range v (which depends on the current weather condition) determines the atmospheric attenuation, and thus significantly affects the achievable data rates of FSO links. Thus, we further analyze how the visibility range v affects the performance of different algorithms. Assuming that  $\zeta = 1$ ,  $\varphi_i = 300$  ms, and the steerable FSO receiver is serving TXs 2, 3, 4, and 5, Figs. 11 and 12 show the average delay of each FSO transmitter and the total average delay of the FSO transmitters, respectively, incurred by different algorithms. From Fig. 11, we can find when v < 4.3 km, none of the algorithms can generate a feasible scheduling because of the low achieve data rates of the FSO links caused by severe atmospheric attenuation. As v increases, the atmospheric attenuation reduces, and so the achievable data rate of each FSO link increases. TWIST is the first algorithm that generates a feasible scheduling as vincreases. Also, the performance (in terms of the average delay of each FSO transmitter and the total average delay of the FSO transmitters) of TWIST is always better than RR



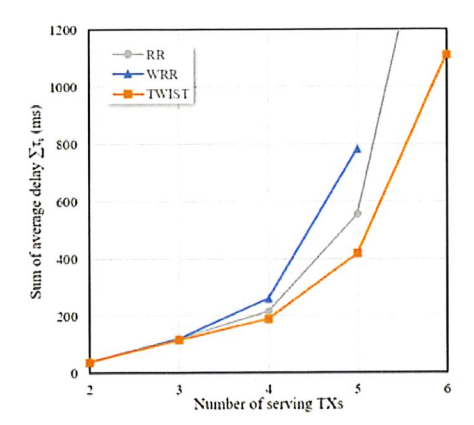


Fig. 13. Sum of average delay over number of serving FSO transmitters.

and WRR. Yet, the performance gaps between TWIST and RR/WRR reduces as  $\boldsymbol{v}$  increases.

We further investigate the performance of the scheduling algorithms under different number of serving FSO transmitters. Assuming  $\xi=1$  and  $\varphi_i=300$  ms, Fig. 13 shows the total average delay of all the serving FSO transmitters by varying the number of serving FSO transmitters. Basically, the steerable FSO receiver serving more FSO transmitters could significantly increase the average delay of each FSO transmitter. From the figure, we can find when the number of serving FSO transmitters is more than 3, TWIST outperforms RR and WRR, and the performance gap increases as the number of serving FSO transmitters increases. Note that RR and WRR are unable to generate a feasible scheduling solution when the number of serving FSO transmitters is 6 and 5, respectively.

Finally, we analyze the complexity of different algorithms by testing the execution time of the algorithms executed by a server (1.8 GHz Intel core i5-8250u CPU and 8 GB memory). As shown in Fig. 14, TWIST always incurs longer execution time than RR and WRR under different number of serving FSO transmitters. However, the execution time of TWIST (<10 ms) is still practical as the scheduling algorithm does not need to be frequently executed. Note that the execution time of TWIST does not monotonically

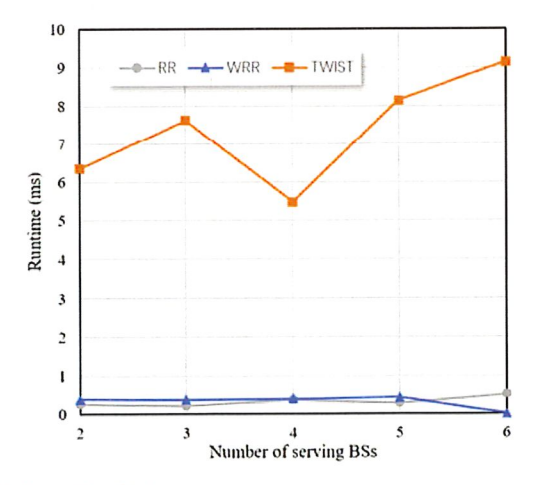


Fig. 12. Sum of average delay over the visibility range.

Fig. 14. Execution time.

Authorized licensed use limited to: UNIVERSITY OF NEW MEXICO. Downloaded on September 15,2023 at 16:24:54 UTC from IEEE Xplore. Restrictions apply.

change when the number of serving FSO transmitters increases. This is because the execution time of TWIST depends on the initial values of  $\boldsymbol{\alpha}^{(0)}$ ,  $\boldsymbol{\beta}^{(0)}$ ,  $\boldsymbol{t}^{(0)}$ , and  $\boldsymbol{H}^{(0)}$  in Algorithm 1. That is, the initial values, which could be a bad estimation that incurs more iterations when the number of serving FSO transmitters is 6, may be a good estimation that incurs fewer number of iterations when the number of serving FSO transmitters is 4.

### 6 CONCLUSION

In this paper, we proposed to apply the steerable FSO system to achieve the communications between the gateway and multiple BSs in order to reduce the capital cost and fully utilize the FSO link capacity. Based on the proposed steerable FSO system, we derived a model to estimate the average delay of transmitting a packet from an FSO transmitter to a steerable FSO receiver in the context of point-to-multipoint communications. The accuracy of the average delay model was validated via simulations. In addition, we formulated the transmission scheduling problem to optimize the active time for each FSO link such that the overall delay of transmitting a packet from the FSO transmitters to the steerable FSO receiver at the gateway is minimized, while satisfying the latency requirements of the FSO transmitters. We designed TWIST to efficiently solve the problem. The performance of TWIST was demonstrated via simulations. Note that the proposed TWIST algorithm can be used not only in the fronthaul/backhaul communications for mobile networks but also in the parallel multi-reconfigurable intelligent surface (RIS) empowered FSO system [41], where an FSO transmitter is equipped with a number of apertures, each of which can transmit an optical beam to an FSO receiver via a RIS. Thus, the FSO receiver has to adjust its direction to receive different optical beams transmitted from different apertures at the FSO transmitter.

In the future, we will develop a steerable FSO testbed to verify the performance of TWIST. The steerable FSO testbed comprises two FSO transmitters and one steerable FSO receiver [42]. An FSO transmitter is consisted of a collimating lens (Thorlab F810FC-1550) mounted on a kinematic platform, a SFP module, a thunderbolt adaptor (QNAP QNA-T310G1S), and a laptop. The laptop is used to generate digital data streams, which are sent to the SFP module via the thunderbolt adaptor. The SFP module is used to generate the optical signals by modulating the data streams. Finally, the collimating lens is to collimate and emit an optical beam, which carries the optical signals, to the FSO receiver. The FSO receiver is consisted of a collimating lens (Thorlab F810FC-1550) mounted on a rotation stage (Thorlab DDR-100), a SFP module, a network interface controller (Intel x520), and a server. The collimating lens is to receive the optical beam sending from an FSO transmitter. The received optical beam is sent to the SFP module, which demodulates digital data streams from the optical signals and sends the digital data streams to the server via the network interface controller. The rotation stage is used to steer the collimating lens of the FSO receiver to receive the optical beams sent from the two FSO transmitters.

REFERENCES

 M. A. Esmail, A. Ragheb, H. Fathallah, and M. Alouini, "Investigation and demonstration of high speed full-optical hybrid FSO/fiber communication system under light sand storm condition," *IEEE Photon. J.*, vol. 9, no. 1, pp. 1–12, Feb. 2017.

[2] H. Zhang, Y. Dong, J. Cheng, M. J. Hossain, and V. C. M. Leung, "Fronthauling for 5G LTE-U ultra dense cloud small cell networks," IEEE Wireless Commun., vol. 23, no. 6, pp. 48–53, Dec. 2016.

[3] I. K. Son and S. Mao, "A survey of free space optical networks," Digit. Commun. Netw., vol. 3, no. 2, pp. 67–77, 2017.

 J. Lian, X. Wang, M. Noshad, and M. Brandt-Pearce, "Optical wireless interception vulnerability analysis of visible light communication system," in *Proc. IEEE Int. Conf. Commun.*, 2018, pp. 1–6.

[5] X. Sun, N. Ansari, and R. Fierro, "Jointly optimized 3D drone mounted base station deployment and user association in drone assisted mobile access networks," *IEEE Trans. Veh. Technol.*, vol. 69, no. 2, pp. 2195–2203, Feb. 2020.

[6] D. Wu, X. Sun, and N. Ansari, "An FSO-based drone assisted mobile access network for emergency communications," *IEEE Trans. Natur. Sci. Eng.*, vol. 7, no. 3, pp. 1597–1606, Jul.—Sep. 2020.

Trans. Netw. Sci. Eng., vol. 7, no. 3, pp. 1597–1606, Jul.–Sep. 2020.

S. Zhang, X. Sun, and N. Ansari, "Placing multiple drone base stations in hotspots," in Proc. IEEE 39th Sarnoff Symp., Sep. 2018, pp. 1–6.

[8] D. Wu, X. Sun, and N. Ansari, "A cooperative drone assisted mobile access network for disaster emergency communications," in *Proc. IEEE Global Commun. Conf.*, 2019, pp. 1–6.

[9] M. Curran et al., "FSONet: A wireless backhaul for multi-gigabit picocells using steerable free space optics," in Proc. 23rd Annu. Int. Conf. Mobile Comput. Netw., 2017, pp. 154–166.

[10] T. Liu, H.-l. Zhang, H.-h. Fu, P. Wang, and N. Xiang, "Performance analysis of multiuser diversity scheduling schemes in FSO communication system," Optoelectron. Lett., vol. 14, no. 4, pp. 296–300, 2018.

[11] FS United States, "SFP-10G-ZR datasheet." Accessed: Mar. 30, 2020. [Online]. Available: https://img-en.fs.com/file/datasheet/10g-base-zr-80km.pdf

[12] Thorlabs, "Achromatic fiber collimator C810FC," Accessed: Mar. 30, 2020. [Online]. Available: https://www.thorlabs.com/thorproduct.cfm?partnumber=C80FC-C

thorproduct.cfm?partnumber=C80FC-C

[13] B. A. Bjerke, "LTE-advanced and the evolution of LTE deployments," *IEEE Wirel. Commun.*, vol. 18, no. 5, pp. 4–5, Oct. 2011

[14] M. Curran and H. Gupta, "Providing line-of-sight in a free-space-optics based data center architecture," in Proc. IEEE Int. Conf. Commun., 2016, pp. 1–7.

[15] M. Ghobadi et al., "ProjecToR: Agile reconfigurable data center interconnect," in Proc. ACM SIGCOMM Conf., 2016, pp. 216–229.

[16] P. Deng, M. Kavehrad, and Y. Lou, "MEMS-based beam-steerable FSO communications for reconfigurable wireless data center," in Proc. SPIE Broadband Access Commun. Technol. XI, pp. 33–41, 2017.

[17] M. Najafi, H. Ajam, V. Jamali, P. D. Diamantoulakis, G. K. Karagiannidis, and R. Schober, "Statistical modeling of FSO fronthaul channel for drone-based networks," in *Proc. IEEE Int. Conf. Commun.*, 2018, pp. 1–7.

[18] M. Z. Hassan, M. J. Hossain, J. Cheng, and V. C. M. Leung, "Joint FSO fronthaul and millimeter-wave access link optimization in cloud small cell networks: A statistical-QOS aware approach," *IEEE Trans. Commun.*, vol. 67, no. 6, pp. 4208–4226, Jun. 2019.
 [19] N. Ansari, Q. Fan, X. Sun, and L. Zhang, "SoarNet," *IEEE Wirel*.

 N. Ansari, Q. Fan, X. Sun, and L. Zhang, "SoarNet," IEEE Wirel. Commun., vol. 26, no. 6, pp. 37–43, Dec. 2019.
 S. Song, Y. Liu, L. Guo, and Q. Song, "Optimized relaying and

20] S. Song, Y. Liu, L. Guo, and Q. Song, "Optimized relaying and scheduling in cooperative free space optical fronthaul/backhaul of 5G," Opt. Switching Netw., vol. 30, pp. 62–70, 2018.

[21] N. Ansari, D. Wu, and X. Sun, "FSO as backhaul and energizer for drone-assisted mobile access networks," ICT Exp., vol. 6, no. 2, pp. 139–144, 2020.

[22] P. F. McManamon and A. Ataei, "Progress and opportunities in optical beam steering," in Proc. SPIE Quantum Sensing Nano Electron. Photon., 2019, pp. 109–129.

[23] M. Alzenad, M. Z. Shakir, H. Yanikomeroglu, and M. Alouini, "FSO-based vertical backhaul/fronthaul framework for 5G+ wireless networks," *IEEE Commun. Mag.*, vol. 56, no. 1, pp. 218–224, Jan. 2018.

[24] Z. Gu, J. Zhang, Y. Ji, L. Bai, and X. Sun, "Network topology reconfiguration for FSO-based fronthaul/backhaul in 5G+ wireless networks," *IEEE Access*, vol. 6, pp. 69426–69437, 2018.

Authorized licensed use limited to: UNIVERSITY OF NEW MEXICO. Downloaded on September 15,2023 at 16:24:54 UTC from IEEE Xplore. Restrictions apply.

[25] Z. Gu, J. Zhang, X. Sun, and Y. Ji, "Optimizing networked flying platform deployment and access point association in FSO-based fronthaul networks," IEEE Wireless Commun. Lett., vol. 9, no. 8, pp. 1221-1225, Aug. 2020.

Q. Fan et al., "Reducing the impact of handovers in ground-totrain free space optical communications," IEEE Trans. Veh. Tech-

nol., vol. 67, no. 2, pp. 1292–1301, Feb. 2018.
[27] M. S. Rahman, K. Zheng, and H. Gupta, "FSO-VR: Steerable free space optics link for virtual reality headsets," in Proc. 4th ACM Workshop Weamble Syst. Appl., 2018, pp. 11-15.
[28] N. Hamedazimi et al., "FireFly: A reconfigurable wireless data

center fabric using free-space optics," Comput. Commun. Rev., vol. 44, no. 4, pp. 319–330, 2014.

[29] I. Khader, H. Bergeron, L. C. Sinclair, W. C. Swann, N. R. Newbury, and J.-D. Deschênes, "Time synchronization over a freespace optical communication channel," Optica, vol. 5, no. 12, pp. 1542-1548, 2018.

I. I. Kim, B. McArthur, and E. J. Korevaar, "Comparison of laser beam propagation at 785 nm and 1550 nm in fog and haze for optical wireless communications," in Proc. Opt. Wireless Commun. III,

[31] A. C. Motlagh, V. Ahmadi, Z. Ghassemlooy, and K. Abedi, "The effect of atmospheric turbulence on the performance of the free space optical communications," in Proc. 6th Int. Symp. Commun. Syst., Netw. Digit. Signal Process., 2008, pp. 540–543.

[32] L. Yang, X. Gao, and M. Alouini, "Performance analysis of free-

space optical communication systems with multiuser diversity over atmospheric turbulence channels," *IEEE Photon. J.*, vol. 6, no.

2, pp. 1-17, Apr. 2014.

[33] A. A. Farid and S. Hranilovic, "Outage capacity optimization for free-space optical links with pointing errors," J. Lightw. Technol., vol. 25, no. 7, pp. 1702-1710, 2007.

[34] R. Liao, "Fading pdf of free-space optical communication system with pointing error," Ph.D. dissertation, Dept. Elect. Comput. Eng., Michigan Technological Univ., Houghton, MI, USA, 2011.

[35] G.-y. Hu, C.-y. Chen, and Z.-q. Chen, "Free-space optical communication using visible light," J. Zhejiang Univ.-Sci. A, vol. 8, no. 2, pp. 186–191, 2007. K. Schittkowski, "NLPQL: A fortran subroutine solving con-

strained nonlinear programming problems," Ann. Operations Res.,

vol. 5, no. 2, pp. 485–500, 1986.
[37] J. Ford and I. Moghrabi, "Multi-step quasi-newton methods for optimization," J. Comput. Appl. Math., vol. 50, no. 1-3, pp. 305-323,

[38] P. T. Boggs and J. W. Tolle, "Sequential quadratic programming,"

Acta Numerica, vol. 4, no. 1, pp. 1–51, 1995.
[39] L. Lukšan and E. Spedicato, "Variable metric methods for unconstrained optimization and nonlinear least squares," J. Comput. Appl. Math., vol. 124, no. 1/2, pp. 61–95, 2000.

[40] H. Chaskar and U. Madhow, "Fair scheduling with tunable

latency: A round-robin approach," IEEE/ACM Trans. Netw., vol.

 11, no. 4, pp. 592–601, Aug. 2003.
 [41] A.-A. A. Boulogeorgos, N. Chatzidiamantis, H. G. Sandalidis, A. Alexiou, and M. Di Renzo, "Cascaded composite turbulence and misalignment: Statistical characterization and applications to reconfigurable intelligent surface-empowered wireless systems, 2021, ar Xiv:2106.15082.

[42] SECNet, "Steerable FSO testbed," Accessed: Dec. 3, 2020. [Online]. Available: http://www.unm.edu/sunxiang/index.htm



Xiang Sun (Member, IEEE) received the BE and ME degrees from the Hebei University of Engineering in 2011 and 2008, respectively, and the PhD degree in electrical engineering from the New Jersey Institute of Technology (NJIT) in 2018. He is currently an assistant professor with the Department of Electrical and Computer Engineering, University of New Mexico. His research interests include free space optics, wireless networks, distributed/cooperative machine learning, Internet of Things, edge computing, and green

communications and computing. He was the recipient of several honors and awards, including the NJIT Ross Fellowship 2014-2015, 2016 IEEE International Conference on Communications (ICC) Best Paper Award, 2017 IEEE Communications Letters Exemplary Reviewers Award, the 2018 NJIT Hashimoto Prize, 2018 InterDigital Innovation Award on IoT Semantic Mashup, and the 2019 IEICE Communications Society Best Tutorial Paper Award. He is an associate editor for the IEEE Open Journal of the Computer Society and the Elsevier Digital Communications and Networks.



Liangkun Yu (Graduate Student Member, IEEE) received the BS and MS degrees in communications engineering from Fuzhou University, Fuzhou. China, in 2014 and 2017, respectively. He is currently working toward the doctoral degree with the SENet Lab, University of New Mexico. His research interests include concentration on federated learning (FL), free space optics (FSO), nonorthogonal multiple access (NOMA), and drone-assisted mobile access networks.



Tianrun Zhang (Graduate Student Member, IEEE) received the BS degree in 2019 in electrical engineering from the University of New Mexico, New Mexico, USA, where he is currently working toward the PhD degree in computer engineering. His research interests include FSO, wireless networks, and Internet of Things.

▷ For more information on this or any other computing topic, please visit our Digital Library at www.computer.org/csdl.